



Contact-reactive brazing mechanism of $\text{Al}_{0.3}\text{CoCrFeNi}$ high-entropy alloys using a niobium interlayer

Yu Lei¹ · Yi-nan Li¹ · Xiao-guo Song² · Sheng-peng Hu² · Wei-min Long³ · Hai-chuan Shi⁴ · Zu-bin Chen⁵

Received: 30 April 2024 / Revised: 24 June 2024 / Accepted: 29 June 2024
© China Iron and Steel Research Institute Group Co., Ltd. 2024

Abstract

The contact-reactive brazing of $\text{Al}_{0.3}\text{CoCrFeNi}$ high-entropy alloys with a Nb interlayer was researched. The effects of Nb thickness and brazing temperature on the interfacial microstructure and mechanical properties of $\text{Al}_{0.3}\text{CoCrFeNi}$ joints were investigated. The results show that with Nb thickness increasing from 10 to 100 μm , the average width of $\text{Al}_{0.3}\text{CoCrFeNi}$ joints is increased from 127 to 492 μm and the erosion volume of $\text{Al}_{0.3}\text{CoCrFeNi}$ base metals (BMs) by face-centered cubic-Nb eutectic liquid is enlarged accordingly. With increasing brazing temperature from 1280 to 1360 $^{\circ}\text{C}$, the intergranular penetration of eutectic liquid into $\text{Al}_{0.3}\text{CoCrFeNi}$ BMs becomes more severe and lamellar Laves phase is broken-up and spherized. The shear strength of joint is increased gradually from 374 to 486 MPa and then decreased to 475 MPa. The maximum shear strength value of 486 MPa is obtained when brazing at 1340 $^{\circ}\text{C}$ for 10 min, reaching about 78% of the shear strength of $\text{Al}_{0.3}\text{CoCrFeNi}$ BMs. Besides, the brazing mechanism was analyzed in details.

Keywords Contact-reactive brazing · High-entropy alloy · Intergranular penetration · Shear strength · Mechanism

1 Introduction

Compared to traditional metallic materials, $\text{Al}_{0.3}\text{CoCrFeNi}$ high-entropy alloys (HEAs) exhibit exceptional strength and ductility at cryogenic temperatures due to its lower

stacking fault energy [1–3]. Study on the brazing of $\text{Al}_{0.3}\text{CoCrFeNi}$ HEAs to itself can promote the fabrication and cryogenic temperatures application of $\text{Al}_{0.3}\text{CoCrFeNi}$ components with complex geometrical shape. Up to now, many conventional Ni-based [4–6], Ag-based [7–9] and Au-based [10] brazing filler metals have been developed to braze HEAs, but the metallurgical compatibility between the braze zone and HEAs base metals (BMs) is poor. To address this issue, we exploit the contact-reactive brazing of $\text{Al}_{0.3}\text{CoCrFeNi}$ HEAs with a pure Nb interlayer [11], the face-centered cubic (FCC)-Nb filling liquid produced by the eutectic reaction between $\text{Al}_{0.3}\text{CoCrFeNi}$ HEAs and Nb foil transforms to a Laves/FCC[Nb]ss eutectic structure in the brazing seam, which exhibits a superior compatibility with $\text{Al}_{0.3}\text{CoCrFeNi}$ BMs. Hence, the $\text{Al}_{0.3}\text{CoCrFeNi}$ joint presents a balanced strength and ductility at both room and cryogenic temperatures. Nevertheless, it is still a lack of detail studies on the main controlling process of $\text{Al}_{0.3}\text{CoCrFeNi}$ HEAs/Nb contact-reactive brazing and the formation mechanism of Laves/FCC[Nb]ss eutectic structure. In this paper, the influences of Nb interlayer thickness and brazing temperature on the interfacial microstructure and mechanical properties of $\text{Al}_{0.3}\text{CoCrFeNi}$ joints are

✉ Yu Lei
leiyu@qut.edu.cn

✉ Sheng-peng Hu
sp_hu@hit.edu.cn

¹ School of Mechanical and Automotive Engineering, Qingdao University of Technology, Qingdao 266000, Shandong, China

² State Key Laboratory of Precision Welding and Joining of Materials and Structures, Harbin Institute of Technology, Harbin 150001, Heilongjiang, China

³ State Key Laboratory of Advanced Brazing Filler Metals and Technology, Zhengzhou Research Institute of Mechanical Engineering, Zhengzhou 450001, Henan, China

⁴ School of Materials Science and Engineering, Shanghai University of Engineering Science, Shanghai 201620, China

⁵ Yantai Research Institute, Harbin Engineering University, Yantai 264006, Shandong, China

investigated. The formation mechanism of Laves/FCC[Nb]ss eutectic structure is discussed in details. This research will further enrich the theoretical basis for the contact-reactive brazing of $\text{Al}_{0.3}\text{CoCrFeNi}$ HEAs and is expected to promote the fabrication and cryogenic application of complex $\text{Al}_{0.3}\text{CoCrFeNi}$ HEAs components.

2 Experimental

$\text{Al}_{0.3}\text{CoCrFeNi}$ HEAs plate with a dimension of $100\text{ mm} \times 100\text{ mm} \times 6\text{ mm}$ was prepared by using electromagnetic levitation melt centrifugal casting (ELCC) method. After solid solution treatment at $1200\text{ }^\circ\text{C}$ for 4 h, the plate was cold-rolled into a thin sheet with total thickness reduction of $\sim 50\%$, followed by a subsequent recrystallization at $1100\text{ }^\circ\text{C}$ for 1 h. As reported in previous work [12], $\text{Al}_{0.3}\text{CoCrFeNi}$ BMs are an FCC-structured solid solution including equiaxed crystals, fine-scale recrystallized grains and annealing twins, and its average shear strength is about 625 MPa. $\text{Al}_{0.3}\text{CoCrFeNi}$ sheet was tailored into several pieces with a dimension of $12\text{ mm} \times 12\text{ mm} \times 2.5\text{ mm}$ by wire electrical discharge machining. All the faying surfaces were ground using SiC sandpapers with the grit size range of 600–2000. Nb foils with a thickness range of 10–100 μm were cut into $12\text{ mm} \times 12\text{ mm}$ slices as the interlayers. Prior to brazing, all the $\text{Al}_{0.3}\text{CoCrFeNi}$ BMs and Nb interlayers were ultrasonically cleaned in acetone for 15 min to remove the pollutants and oxides. Afterward, $\text{Al}_{0.3}\text{CoCrFeNi}/\text{Nb}/\text{Al}_{0.3}\text{CoCrFeNi}$ were assembled like a “sandwich” structure. Brazing experiments were performed at the temperature range of $1240\text{--}1360\text{ }^\circ\text{C}$ for 10 min in a vacuum of 3.0×10^{-3} Pa. A pressure of 0.25 kPa was exerted on the assembly to ensure close contact during brazing. The brazed sample was cut into four pieces of $5\text{ mm} \times 5\text{ mm}$ perpendicularly for microstructure examination and shear strength test, as reported in Ref. [12]. Before microstructure observation, the sample needs to be ground and polished using SiC sandpapers with the grit sizes ranging from 400 to 3000. Interfacial microstructure of brazed joints was characterized using a field emission scanning electron microscope (FE-SEM, MERLIN Compact, ZEISS) equipped with an energy dispersive spectrometer (EDS). Shear strength test was performed using an INSTRON 5967 at a displacement velocity of 0.5 mm/min. Before testing, the sample needs to be placed in a self-prepared shear apparatus [12]. More than three specimens were tested for the same conditions to keep the data reliability. The fracture path and fracture morphologies of joints were analyzed by SEM and X-ray diffraction (XRD).

3 Results and discussion

3.1 Microstructure characterization of $\text{Al}_{0.3}\text{CoCrFeNi}$ joints

Figure 1 shows the interfacial microstructures of $\text{Al}_{0.3}\text{CoCrFeNi}$ joints brazed by a Nb interlayer with different thicknesses at $1300\text{ }^\circ\text{C}$ for 10 min. For the joint brazed with 10 μm -thick Nb interlayer, a few micro-cracks and an obvious gap can be observed in the braze zone. When the thickness of Nb interlayer is equal or exceeds 30 μm , a lamella-like Laves/FCC[Nb]ss eutectic structure forms in the joint, exhibiting a good metallurgical bonding with $\text{Al}_{0.3}\text{CoCrFeNi}$ BMs. With increasing Nb interlayer to 100 μm , the average width of $\text{Al}_{0.3}\text{CoCrFeNi}$ joints is improved from 127 to 492 μm accordingly. When brazing with an 80 μm -thick Nb interlayer, the dissolution volume of $\text{Al}_{0.3}\text{CoCrFeNi}$ BMs by the eutectic liquid phase is enlarged notably and a few proeutectic FCC[Nb]ss phases are precipitated before Laves/FCC[Nb]ss isothermal solidification. When Nb interlayer thickness is up to 100 μm , the total dissolution width of $\text{Al}_{0.3}\text{CoCrFeNi}$ BMs is about 392 μm , and the volume fraction of pre-eutectic FCC[Nb]ss phase in the brazing seam is further increased. Actually, the contact-reactive course can be controlled by the thickness of the interlayer [13]. Once the interlayer thickness is more than 100 μm , the erosion extent of the base metal by eutectic liquid phase becomes more severe.

Figure 2 shows the interfacial microstructures of $\text{Al}_{0.3}\text{CoCrFeNi}$ joints brazed with a 30 μm -thick Nb interlayer at the temperature range of $1280\text{--}1360\text{ }^\circ\text{C}$ for 10 min. At $1280\text{ }^\circ\text{C}$, an in-situ eutectic reaction between Nb interlayer and $\text{Al}_{0.3}\text{CoCrFeNi}$ BM is triggered. The intergranular penetration of eutectic FCC-Nb liquid into $\text{Al}_{0.3}\text{CoCrFeNi}$ BM is slight. With increasing the brazing temperature, the intergranular infiltration becomes more severe. Figure 3 shows the average width of bonding zone and braze zone as a function of brazing temperature. When brazing at $1280\text{ }^\circ\text{C}$, the average width of the braze zone with a Laves/FCC[Nb]ss eutectic structure is about 165 μm . Due to a relatively low diffusion coefficient of Nb atoms in $\text{Al}_{0.3}\text{CoCrFeNi}$ BMs at $1280\text{ }^\circ\text{C}$, the diffusion distance of Nb atoms in $\text{Al}_{0.3}\text{CoCrFeNi}$ BMs is limited. Thus, the total width of bonding zone is about 265 μm . With increasing the brazing temperature, the average width of braze zone is significantly decreased from 165 to 25 μm , while that of bonding zone is decreased firstly and then gradually increased to 214 μm at $1360\text{ }^\circ\text{C}$ due to the increased diffusion coefficient of Nb atoms in $\text{Al}_{0.3}\text{CoCrFeNi}$ BMs.

Figure 4 shows the partial enlarged microstructures of $\text{Al}_{0.3}\text{CoCrFeNi}$ joints brazed at a temperature range of $1280\text{--}1360\text{ }^\circ\text{C}$ for 10 min. It can be seen that a few white

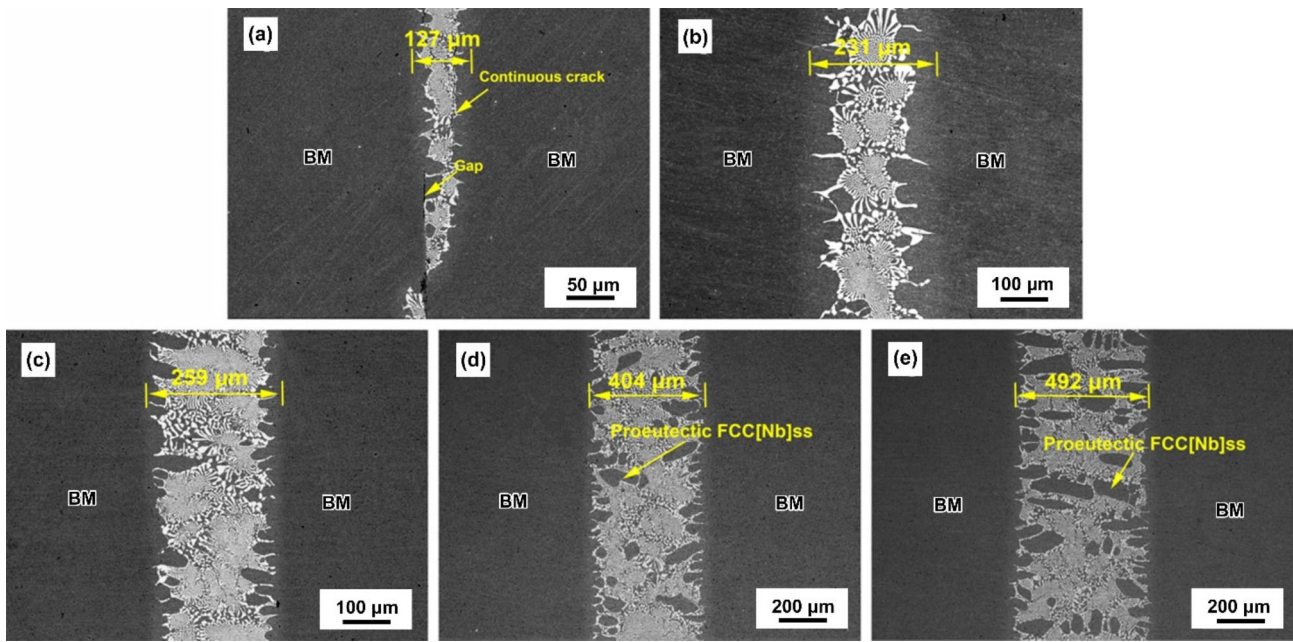


Fig. 1 Interfacial microstructures of $\text{Al}_0.3\text{CoCrFeNi}$ joints brazed with different Nb interlayers at 1300 °C for 10 min. **a** 10 μm ; **b** 30 μm ; **c** 50 μm ; **d** 80 μm ; **e** 100 μm

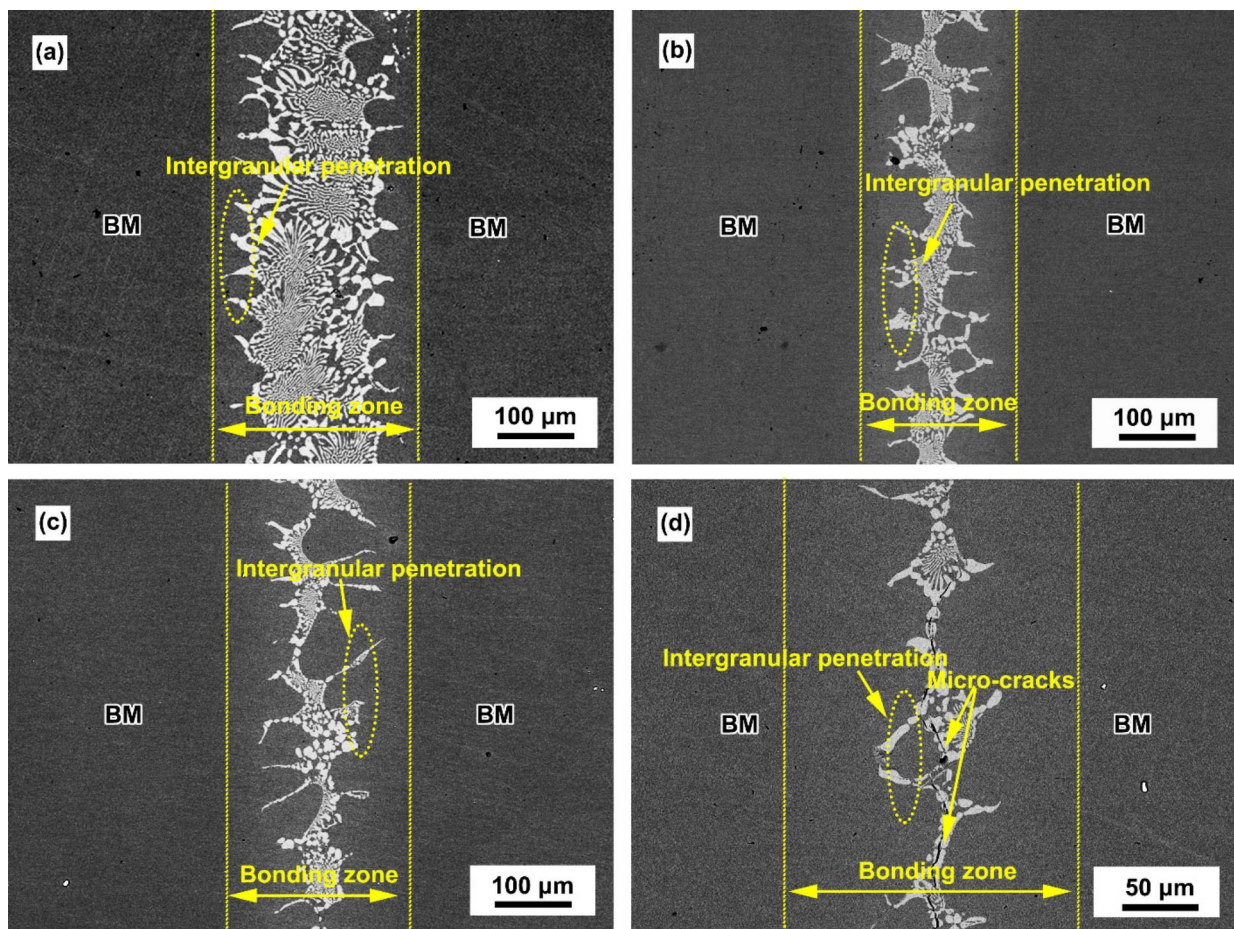


Fig. 2 Effect of brazing temperature on interfacial microstructure of $\text{Al}_0.3\text{CoCrFeNi}$ joints. **a** 1280 °C; **b** 1320 °C; **c** 1340 °C; **d** 1360 °C

Nb(s,s) emerge at the grain boundaries of Laves/FCC[Nb]ss eutectic colonies at 1280 °C. When the brazing temperature reaches or exceeds 1320 °C, lamellar Laves phase is broken-up and spherized. A few black precipitations (point A and point B) can be found at the Laves/FCC interface, as shown in Fig. 4c, d. According to the EDS results listed in Table 1 and Ni–Al binary alloy phase diagram [14], the black phase is determined as B2-NiAl

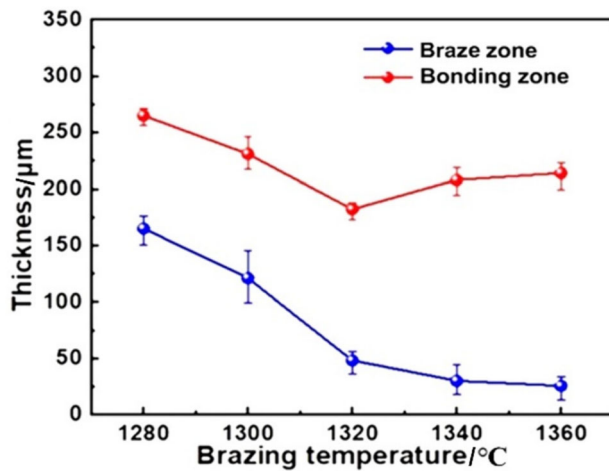


Fig. 3 Effect of brazing temperature on widths of bonding zone and braze zone

intermetallic. The brazing seam is further narrowed at 1360 °C and several micro-cracks occur in the Laves phase or at the Laves/FCC[Nb]ss interface. The residual thermal stress σ value [15] between dissimilar materials can be estimated by Eq. (1):

$$\sigma = \frac{E_A \times E_B}{E_A + E_B} (\alpha_A - \alpha_B) \times \Delta T \quad (1)$$

where E is elastic modulus, GPa; α is thermal expansion coefficient, K^{-1} ; ΔT refers to temperature difference, °C; and subscripts A and B represent phase A and phase B, respectively. α of $\text{Al}_{0.3}\text{CoCrFeNi}$ HEAs is about 0.974×10^{-5} – $1.58 \times 10^{-5} \text{ K}^{-1}$ [16], while that of C14 Laves phase is 0.25×10^{-5} – $0.4 \times 10^{-5} \text{ K}^{-1}$ at the temperature range of 27–927 °C [17]. When brazing temperature is up to 1360 °C, the residual thermal stress at the Laves/FCC interface is increased inevitably during the cooling process. Consequently, several micro-cracks initiate at the Laves/FCC interface where a large deformation difference exists between hard Laves and soft FCC phase, and further propagate in the brittle Laves phase. As the crack tip can be passivated by the soft FCC phase, the propagation paths of these micro-cracks are deflected as denoted in Fig. 4d. In addition, the embrittlement of the Laves/FCC interface where B2-phase precipitates out also causes the initiation and propagation of micro-cracks.

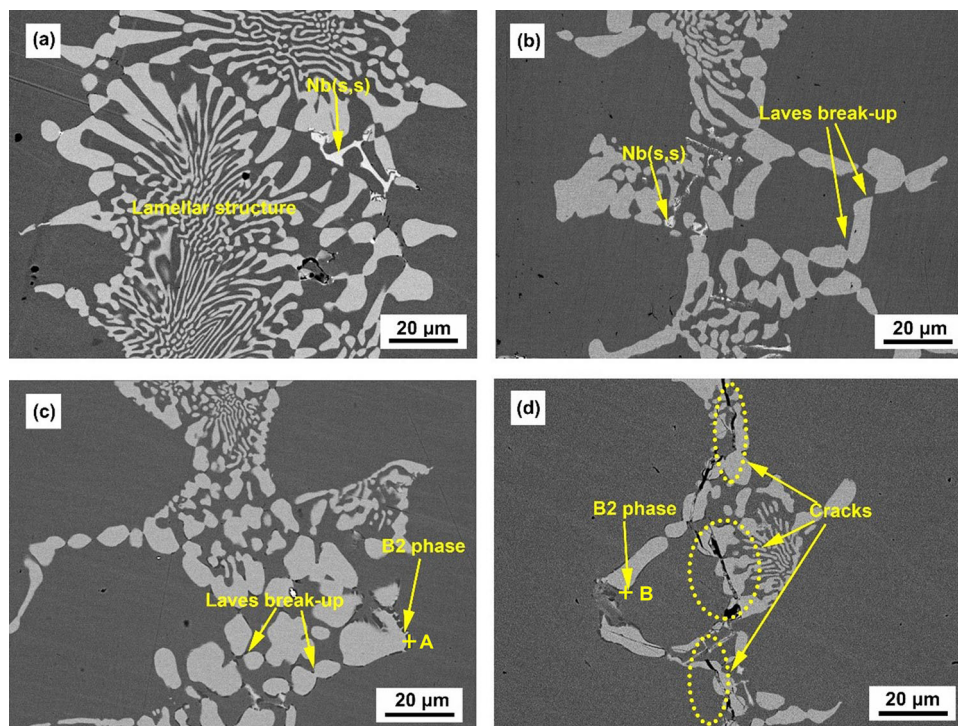
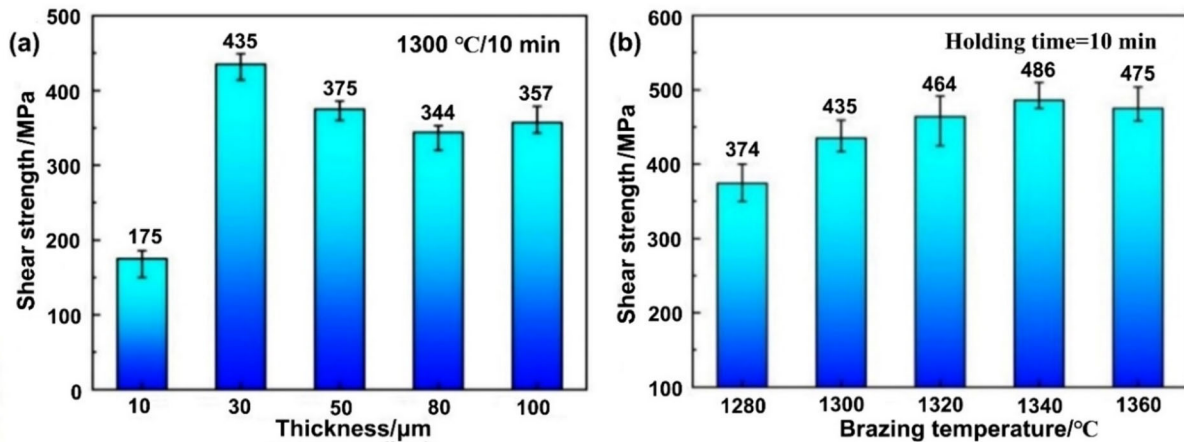


Fig. 4 Effect of brazing temperature on partial microstructures of $\text{Al}_{0.3}\text{CoCrFeNi}$ joints. **a** 1280 °C; **b** 1320 °C; **c** 1340 °C; **d** 1360 °C

Table 1 Chemical compositions of points A and B in Fig. 4

Point	Element/at. %						Possible phase
	Al	Co	Cr	Fe	Ni	Nb	
A	28.18	13.69	11.16	11.05	30.71	5.20	B2
B	25.28	9.40	11.05	15.43	32.52	6.33	B2

**Fig. 5** Shear strengths of Al_{0.3}CoCrFeNi joints obtained at different brazing parameters. **a** Shear strength vs. thickness of Nb interlayer; **b** shear strength vs. brazing temperature

3.2 Mechanical properties of Al_{0.3}CoCrFeNi joints

Figure 5a shows the average room-temperature shear strengths of Al_{0.3}CoCrFeNi joints brazed by using a Nb interlayer with different thicknesses at 1300 °C for 10 min. When brazing with a 10 μm-thick Nb interlayer, the shear strength of joint is only 175 MPa due to the existence of micro-cracks and an obvious gap as shown in Fig. 1a. When Nb thickness is increased to 30 μm, joint shear strength is up to 435 MPa. With further increasing Nb thickness, the joint shear strength is dropped to some extent, which can be ascribed to the decreased shear deformation ability of braze zone. The influence of brazing temperature on the shear strength of joint is displayed in Fig. 5b. With increasing the brazing temperature from 1280 to 1360 °C, the joint shear strength is increased gradually from 374 to 486 MPa and then decreased to 475 MPa. The shear strength reduction at 1360 °C can be attributed to the formation of micro-cracks in the joint. The maximum shear strength value of 486 MPa is obtained when brazing at 1340 °C for 10 min, reaching ~ 78% of the shear strength of Al_{0.3}CoCrFeNi BMs.

The fracture morphology of the joint brazed at 1280 °C for 10 min is shown in Fig. 6, and it can be seen that the joint is mainly ruptured in the eutectic zone in a brittle quasi-cleavage fracture feature, and thus the fracture surface is relatively flat as displayed in Fig. 6a, b. In Fig. 6c, a network

tearing edge of soft FCC[Nb]ss phase can be observed around the cleavage planes of hard Laves phase, which is conducive to improving the fracture toughness of joint. As shown in Fig. 6d, e, the fractograph of the joint brazed at 1340 °C for 10 min is uneven and many bumps can be observed. Figure 6f shows the local magnification image of the region where bumps concentrated. It can be seen that several blocky FCC[Nb]ss grains suffer a large degree of plastic deformation and brittle Laves compounds mainly distribute in the grain boundary region of FCC[Nb]ss, which indicates that the joint ruptured in an intergranular fracture mode. During shear deformation stage, many micro-cracks nucleate at the Laves/FCC interface and further propagate in the Laves phase at both the braze zone and intergranular infiltration region. The more the fracture path deflection happens at the intergranular infiltration region, the more the energy consumption is needed during shear fracture [18]. Hence, joint shear strength reaches the maximum value of 486 MPa.

3.3 Contact-reactive brazing mechanism

The contact-reactive brazing mechanism of Al_{0.3}CoCrFeNi joints with pure Nb interlayer is investigated in details. Figure 7a indicates that the interdiffusion between Al_{0.3}CoCrFeNi HEAs and 30 μm-thick Nb interlayer is faint and Al_{0.3}CoCrFeNi BMs are unbonded at 1240 °C for 10

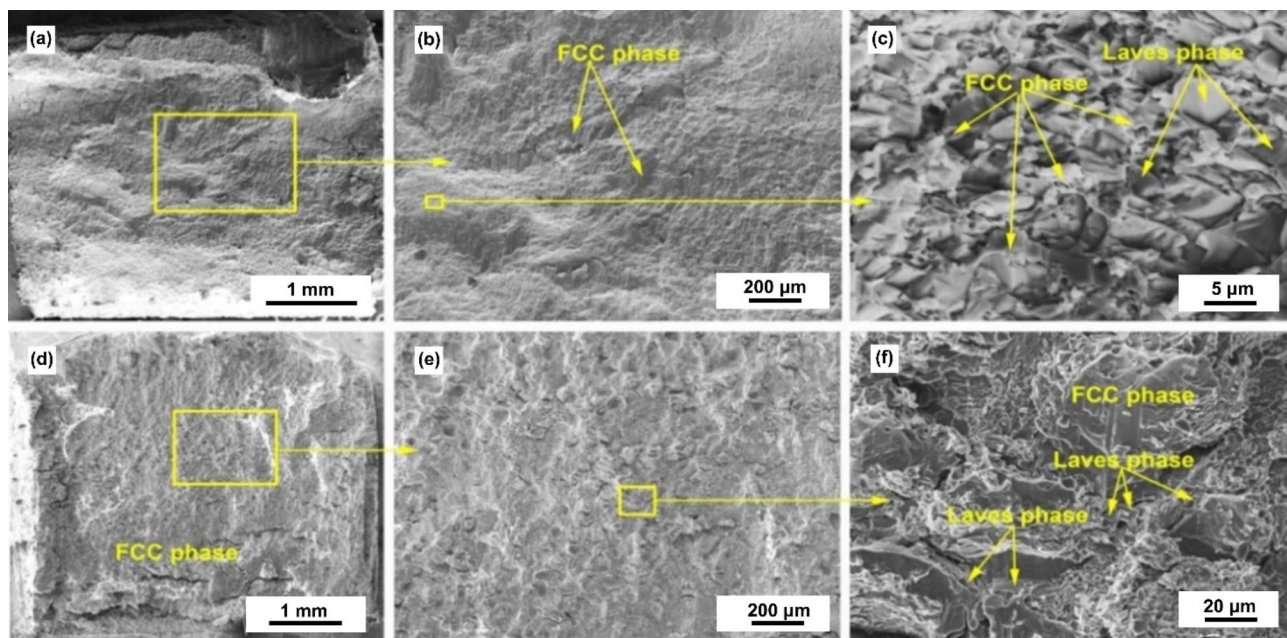


Fig. 6 SEM fractographies of $\text{Al}_{0.3}\text{CoCrFeNi}$ joints brazed at different temperatures for 10 min. **a–c** 1280 °C; **d–f** 1340 °C

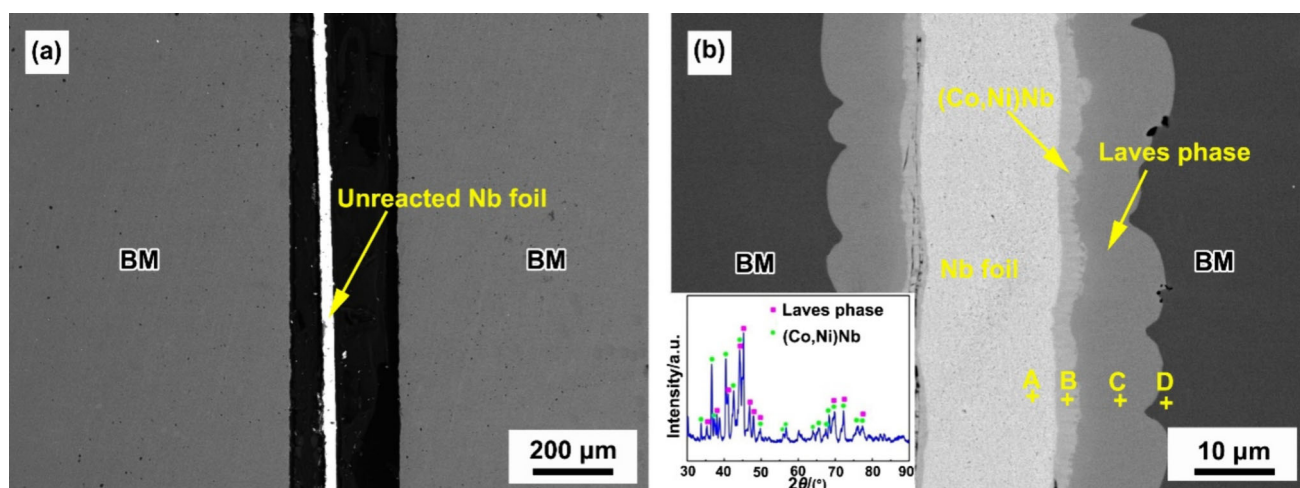


Fig. 7 Interfacial microstructure of $\text{Al}_{0.3}\text{CoCrFeNi}$ joints bonded at different parameters. **a** 1240 °C/10 min; **b** 1260 °C/10 min (inset shows XRD patterns of fracture surface of Nb/ $\text{Al}_{0.3}\text{CoCrFeNi}$ joint)

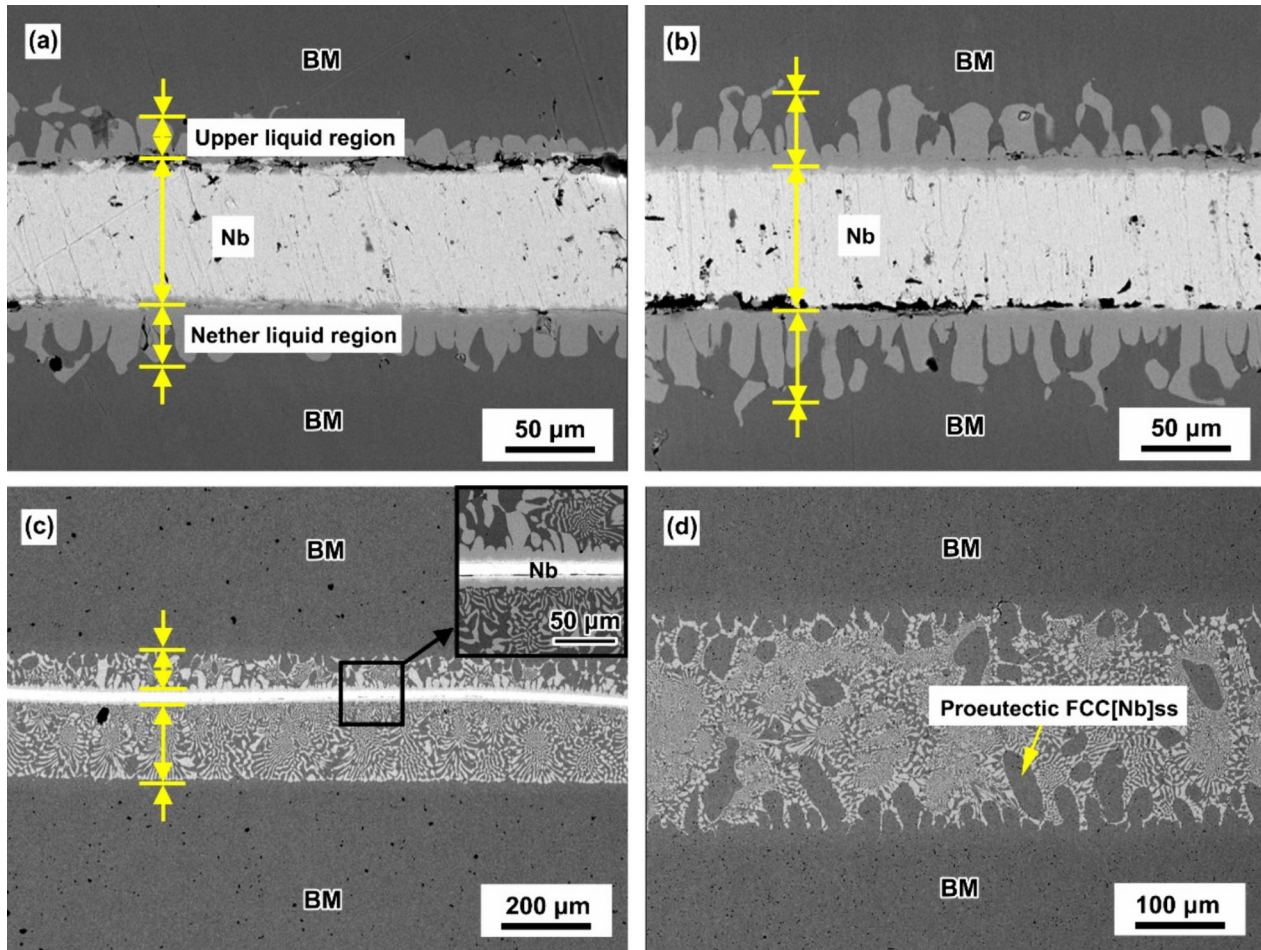
min. When heating at 1240 °C for 10 min, the bonding of $\text{Al}_{0.3}\text{CoCrFeNi}$ BMs can not be realized with a 30 μm -thick Nb interlayer. When the heating temperature is elevated to 1260 °C, two notable diffusion layers form at the Nb/ $\text{Al}_{0.3}\text{CoCrFeNi}$ interface (Fig. 7b). EDS results of points A–D are listed in Table 2. According to the phase diagram of Nb–Co–Ni ternary alloy [19] and the XRD results on the fracture surface of joint (the inset in Fig. 7b), the reaction layer B containing 50.88 at.% Nb, 17.72 at.% Ni and 13.72 at.% Co is determined as (Co, Ni)Nb phase (JCPDS cards 65–7486). The gray reaction layer C containing 24.66 at.% Nb element is determined as a C14-type Laves phase. Al content (8.13 at.%) in point D is higher

than that in the Laves phase (4.86 at.%), which implies that the formation of Laves phase contributes to enhancing the concentration of Al element in FCC phase close to Laves/FCC interface.

When brazing at 1280 °C, the initial eutectic liquid phase between Laves phase and $\text{Al}_{0.3}\text{CoCrFeNi}$ BM generates. Figure 8 shows the interfacial microstructures of the joints brazed with an 80 μm -thick Nb interlayer at 1280 °C for different holding time. In Fig. 8a, $\text{Al}_{0.3}\text{CoCrFeNi}$ brazed joint can be divided into $\text{Al}_{0.3}\text{CoCrFeNi}$ BM, upper liquid phase region, undissolved Nb interlayer, nether liquid phase region and $\text{Al}_{0.3}\text{CoCrFeNi}$ BM. The thickness of (Ni, Co)Nb reaction layer is quite thin and can be

Table 2 Chemical compositions of points A–D in Fig. 7b

Point	Element/at. %						Possible phase
	Al	Co	Cr	Fe	Ni	Nb	
A	–	–	4.68	1.75	–	93.57	Nb(s,s)
B	4.50	13.72	4.04	9.14	17.72	50.88	(Co, Ni)Nb
C	4.86	19.41	17.51	19.40	14.16	24.66	C14 Laves
D	8.13	17.35	23.46	23.43	22.44	5.18	FCC phase

**Fig. 8** Effect of holding time on microstructure of Al_{0.3}CoCrFeNi/Nb/Al_{0.3}CoCrFeNi joints. **a** 30 s; **b** 60 s; **c** 240 s; **d** 480 s

neglected. When the holding time is within 60 s, the dissolution volume of Nb interlayer and the width of eutectic liquid phase are quite limited, as shown in Fig. 8a, b. Figure 8c shows that when the holding time reaches 240 s, the width of unreacted Nb interlayer is dropped obviously and the eutectic liquid phase between unreacted Nb interlayer and Al_{0.3}CoCrFeNi BM is enlarged. The width of upper liquid phase region is narrower than that of nether liquid phase region, which implies that the dissolution velocity between Laves phase and nether Al_{0.3}CoCrFeNi

BM is increased under the force of gravity [20]. When holding for 480 s, Nb interlayer is consumed completely and excess Al_{0.3}CoCrFeNi BM is dissolved by the eutectic liquid (Fig. 8d). During the cooling process, the in-situ formed filling liquid transforms into several proeutectic FCC[Nb]ss + lamellar Laves/FCC[Nb]ss eutectic structure. The contact-reactive brazing mechanism can be divided into three different stages, as illustrated in Fig. 9. (1) Interdiffusion between Nb interlayer and Al_{0.3}CoCrFeNi BMs. During the heating process, the

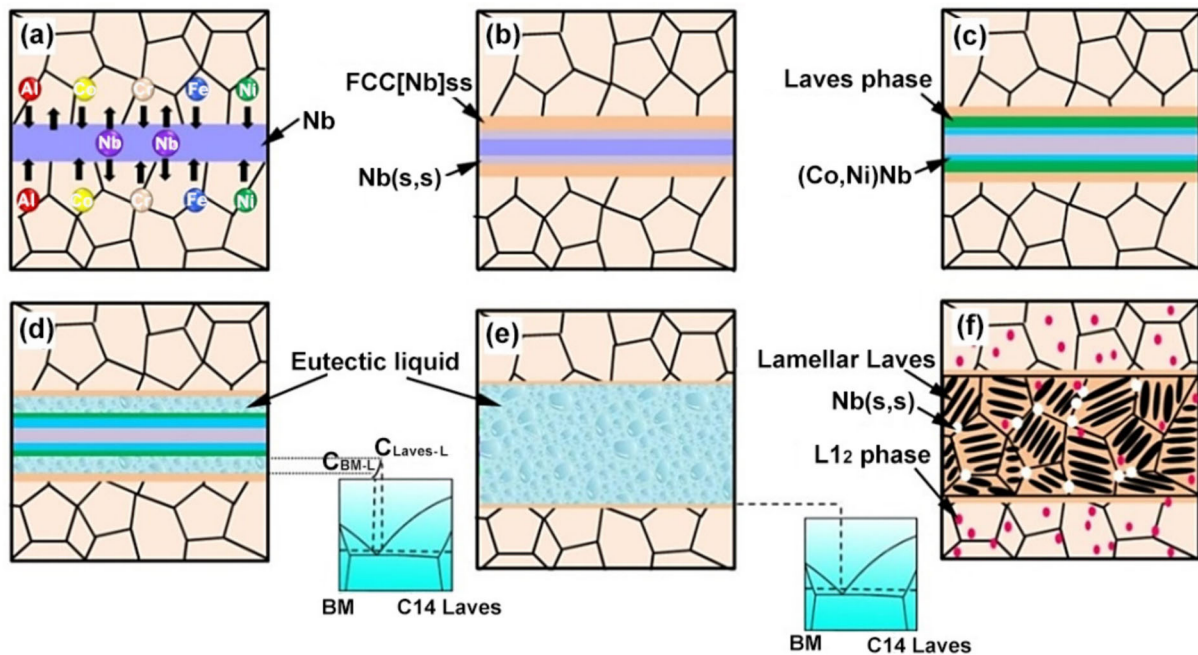


Fig. 9 Schematic diagram of formation mechanism of $\text{Al}_{0.3}\text{CoCrFeNi}$ joint. **a, b** Interdiffusion between Nb and $\text{Al}_{0.3}\text{CoCrFeNi}$ HEAs; **c** formation of Laves and (Co, Ni)Nb reaction layers; **d, e** mutual

dissolution between Nb and $\text{Al}_{0.3}\text{CoCrFeNi}$; **f** formation of Laves/FCC[Nb]ss eutectic structure

interdiffusion between Nb atoms and alloying atoms from $\text{Al}_{0.3}\text{CoCrFeNi}$ BMs is triggered under the concentration gradient, forming a Nb(s,s) and an FCC[Nb]ss diffusion layer, respectively, as illustrated in Fig. 9a, b. With increasing the heating temperature, the FCC[Nb]ss diffusion layer transforms into a C14-type Laves compound layer once the concentration of Nb element in $\text{Al}_{0.3}\text{CoCrFeNi}$ BM exceeds its solid solubility limit. Due to the strong affinity of Co–Nb and Ni–Nb atomic pairs, more Ni and Co atoms diffuse into Nb interlayer preferentially, forming a thin (Ni, Co)Nb reaction layer within Nb side (Fig. 9c). (2) Formation of eutectic liquid phase. When the heating temperature reaches the eutectic temperature of FCC–Nb pseudo binary alloy (between 1260 and 1280 °C), the interface between C14-type Laves phase and FCC[Nb]ss becomes unstable and an initial FCC–Nb eutectic liquid film generates at the Laves/FCC[Nb]ss interface simultaneously (Fig. 9d). As a result, a Nb concentration gradient difference between the Laves/liquid interface ($C_{\text{Laves-L}}$) and the liquid/FCC[Nb]ss interface ($C_{\text{L-FCC[Nb]ss}}$) emerges, which may drive transport of Laves phase toward FCC[Nb]ss, and vice versa. Thus, the width of eutectic liquid is increased steadily until the source of Nb interlayer is exhausted completely, as depicted in Fig. 9e. (3) Isothermal solidification stage. Upon cooling, the FCC–Nb eutectic liquid phase transforms into a lamellar Laves/FCC[Nb]ss eutectic structure (Fig. 9f) by means of the eutectic cooperative nucleation and growth of Laves and FCC phases [21]. Extra Nb atoms can be

excluded from eutectic colonies, leading to a few white Nb(s,s) phases precipitating out in the grain boundaries [22]. Since the formation of Laves/FCC[Nb]ss eutectic structure is an isothermal transformation without a solidification temperature range, the segregation and shrinkage cavity can be alleviated in the braze zone [23]. When brazing at a higher temperature, the diffusion coefficient of Nb atoms in $\text{Al}_{0.3}\text{CoCrFeNi}$ BMs is increased rapidly according to the Arrhenius equation [24]. Since massive Nb atoms prefer to diffuse along the grain boundaries of $\text{Al}_{0.3}\text{CoCrFeNi}$ BMs which have a lower free energy, the enrichment of Nb atoms in the intergranular region induces the eutectic reaction of Nb– $\text{Al}_{0.3}\text{CoCrFeNi}$ BMs and accelerates the dissolution of intergranular region, forming a granular penetration phenomenon. Besides, since the mixing enthalpies of Ni–Al and Ni–Nb atomic pairs are lower than those of other atomic pairs in FCC[Nb]ss and $\text{Al}_{0.3}\text{CoCrFeNi}$ BM, a large number of ordered L1_2 nanoparticles (stoichiometry of $\text{Ni}_3(\text{Al}, \text{Nb})$) are precipitated within both FCC[Nb]ss and $\text{Al}_{0.3}\text{CoCrFeNi}$ BMs, as reported in our previous work [11].

4 Conclusions

1. With increasing Nb interlayer thickness from 10 to 100 μm , the average width of $\text{Al}_{0.3}\text{CoCrFeNi}$ joints is increased from 127 to 492 μm because the erosion of

Al_{0.3}CoCrFeNi BMs by the eutectic liquid becomes more severe. Before isothermal solidification, a few pre-eutectic FCC[Nb]ss phases are precipitated when the thickness of Nb interlayer exceeds 80 μm.

2. With elevating the brazing temperature from 1280 to 1360 °C, the lamellar Laves phase is broken-up and spherized, and the average width of bonding zone is decreased firstly and then gradually increased to 214 μm. The maximum shear strength of Al_{0.3}CoCrFeNi brazed joint is ~ 486 MPa, reaching about 78% of Al_{0.3}CoCrFeNi BM.
3. An initial eutectic liquid film is produced due to the eutectic reaction of Laves + FCC[Nb]ss → L_{Eutectic liquid} at the brazing temperature between 1260 and 1280 °C. Nb concentration gradient difference between the Laves/liquid interface (C_{Laves-L}) and the liquid/FCC[Nb]ss interface (C_{L-FCC[Nb]ss}) drives the transport of Laves phase toward FCC[Nb]ss, and vice versa.

Acknowledgements The authors gratefully acknowledge the financial support from the Outstanding Youth Innovation Team in Universities of Shandong Province (2023KJ114), National Natural Science Foundation of China (Grant No. 52305344), and Natural Science Foundation of Shandong Province, China (Grant No. ZR2022QE073).

Declarations

Conflict of interest The authors declare no conflict of interest.

References

- [1] D. Li, C. Li, T. Feng, Y. Zhang, G. Sha, J.J. Lewandowski, P.K. Liaw, Y. Zhang, *Acta Mater.* 123 (2017) 285–294.
- [2] Q. Li, T.W. Zhang, J.W. Qiao, S.G. Ma, D. Zhao, P. Lu, B. Xu, Z.H. Wang, *Mater. Sci. Eng. A* 767 (2019) 138424.
- [3] D. Li, Y. Zhang, *Intermetallics* 70 (2016) 24–28.
- [4] L. Yuan, J. Xiong, Y. Du, J. Ren, J. Shi, J. Li, *J. Mater. Sci. Technol.* 61 (2021) 176–185.
- [5] C. Lin, R.K. Shiue, S.K. Wu, H.L. Huang, *Entropy* 21 (2019) 283.
- [6] S. Li, J. Li, J. Shi, Y. Du, Y. Peng, F. Jin, J. Xiong, F. Zhang, *Mater. Sci. Eng. A* 804 (2021) 140714.
- [7] G. Wang, G. Sheng, Q. Yu, J. Sun, R. Li, X. Yuan, Y. Zhang, *Mater. Sci. Eng. A* 800 (2021) 140291.
- [8] G. Wang, G. Sheng, Q. Yu, X. Yuan, J. Sun, Y. Jiao, Y. Zhang, *Intermetallics* 126 (2020) 106940.
- [9] G. Wang, G. Sheng, J. Sun, Y. Wei, X. Gao, Z. Yu, X. Yuan, *J. Alloy. Compd.* 829 (2020) 154520.
- [10] C. Lin, R.K. Shiue, S.K. Wu, J.Y. Huang, Y.C. Huang, *Gold Bull.* 53 (2020) 101–109.
- [11] Y. Lei, X. Song, S.P. Hu, W. Fu, D.Y. Lin, T.L. Yang, L.L. Zhu, *Mater. Sci. Eng. A* 835 (2022) 142674.
- [12] Y. Lei, J. Sun, X.G. Song, M.X. Yang, T.L. Yang, J. Yin, *J. Mater. Sci. Technol.* 121 (2022) 245–255.
- [13] L.M. Zhao, Study on contact reactive brazing of magnesium AZ31/aluminum 6061 dissimilar alloys, Dalian University of Technology, Dalian, China, 2007.
- [14] H. Okamoto, M.E. Schlesinger, E.M. Mueller, *ASM Handbook®*, Volume 3, Alloy Phase Diagrams, ASM International, Ohio, USA, 2016.
- [15] Y.Z. Liu, Study on technology and mechanism of brazing C/SiC composite to niobium, Harbin Institute of Technology, Harbin, China, 2007.
- [16] Z. Sun, C. Shi, L. Gao, S. Lin, W. Li, *J. Alloy. Compd.* 901 (2022) 163554.
- [17] L. Rabahi, B. Alili, D. Bradai, T. Grosdidier, A. Kellou, *Intermetallics* 83 (2017) 92–100.
- [18] Q.P. Zhong, Z.H. Zhao, *Fractography*, Higher Education Press, Beijing, China, 2006.
- [19] K.P. Gupta, *J. Phase Equilib. Diffus.* 27 (2006) 173–177.
- [20] C. Yu, M.F. Wu, Z.S. Yu, *Welding Technol.* 33 (2004) 17–18.
- [21] B. Chanda, J. Das, *Adv. Eng. Mater.* 20 (2018) 1700908.
- [22] H. Jiang, L. Jiang, D. Qiao, Y. Lu, T. Wang, Z. Cao, T. Li, *J. Mater. Sci. Technol.* 33 (2017) 712–717.
- [23] Y. Lu, Y. Dong, S. Guo, L. Jiang, H. Kang, T. Wang, B. Wen, Z. Wang, J. Jie, Z. Cao, H. Ruan, T. Li, *Sci. Rep.* 4 (2014) 6200.
- [24] C.A. Sierra, *Biogeochemistry* 108 (2012) 1–15.

Springer Nature or its licensor (e.g. a society or other partner) holds exclusive rights to this article under a publishing agreement with the author(s) or other rightsholder(s); author self-archiving of the accepted manuscript version of this article is solely governed by the terms of such publishing agreement and applicable law.